

# The Structural Basis of Endocannabinoid Oxygenation by Cyclooxygenase-2<sup>\*[5]</sup>

Received for publication, February 11, 2011, and in revised form, March 28, 2011. Published, JBC Papers in Press, April 13, 2011, DOI 10.1074/jbc.M111.230367

Alex J. Vecchio and Michael G. Malkowski<sup>1</sup>

From the Hauptman-Woodward Medical Research Institute and the Department of Structural Biology, The State University of New York, Buffalo, New York, 14203

The cyclooxygenases (COX-1 and COX-2) oxygenate arachidonic acid (AA) in the committed step of prostaglandin biogenesis. Substitutions of I434V, H513R, and I523V constitute the only differences in residues lining the cyclooxygenase channel between COX-1 and COX-2. These changes create a hydrophobic pocket in COX-2, with Arg-513 located at the base of the pocket, which has been exploited in the design of COX-2-selective inhibitors. Previous studies have shown that COX-2, but not COX-1, can oxygenate endocannabinoid substrates, including 2-arachidonoyl glycerol (2-AG). To investigate the isoform-specific structural basis of endocannabinoid binding to COX-2, we determined the crystal structure of the 2-AG isomer 1-arachidonoyl glycerol (1-AG) in complex with wild type and R513H murine ( $\mu$ ) COX-2 to 2.2 and 2.35 Å, respectively, and R513H muCOX-2 in complex with AA to 2.45 Å resolution. The 2,3-dihydroxypropyl moiety of 1-AG binds near the opening of the cyclooxygenase channel in the space vacated by the movement of the Leu-531 side chain, validating our previous hypothesis implicating the flexibility of the Leu-531 side chain as a determinant for the ability of COX-2 to oxygenate endocannabinoid substrates. Functional analyses carried out to complement our structural findings indicated that Y355F and R513H muCOX-2 constructs had no effect on the oxygenation of 1-AG and 2-AG, whereas substitutions that resulted in a shortened side chain for Leu-531 had only modest effects. Both AA and 1-AG bind to R513H muCOX-2 in conformations similar to those observed in the co-crystal structures of these substrates with wild type enzyme.

The reaction catalyzed by the cyclooxygenase enzymes (COX-1 and COX-2),<sup>2</sup> in which prostaglandin H<sub>2</sub> (PGH<sub>2</sub>) is

<sup>\*</sup> This work was supported, in whole or in part, by National Institutes of Health Grant R01 GM077176. This work was also supported by an Arthritis Investigator Award from the Arthritis Foundation as part of the Segal Osteoarthritis Initiative. This work is also based upon research conducted at the Cornell High Energy Synchrotron Source, which is supported by the National Science Foundation under Award DMR-0225180, using the macromolecular diffraction facility at the Cornell High Energy Synchrotron Source, which is supported by Award RR-01646 from the National Institutes of Health through the National Center for Research Resources.

The atomic coordinates and structure factors (codes 3MDL, 3OLT, and 3OLU) have been deposited in the Protein Data Bank, Research Collaboratory for Structural Bioinformatics, Rutgers University, New Brunswick, NJ (<http://www.rcsb.org/>).

<sup>[5]</sup> The on-line version of this article (available at <http://www.jbc.org>) contains supplemental Tables S1–S6 and Figs. S1–S6.

<sup>1</sup> To whom correspondence should be addressed: Hauptman-Woodward Medical Research Institute, 700 Ellicott St., Buffalo, NY 14203. Tel.: 716-898-8624; Fax: 716-898-8660; E-mail: [malkowski@hwi.buffalo.edu](mailto:malkowski@hwi.buffalo.edu).

<sup>2</sup> The abbreviations used are: COX, cyclooxygenase; PG, prostaglandin; AA, arachidonic acid; 1-AG, 1-arachidonoyl glycerol; 2-AG, 2-arachidonoyl

generated from the fatty acid substrate arachidonic acid (AA), represents the committed step in the biosynthesis of prostaglandins and thromboxanes (reviewed in Refs. 1 and 2). Downstream synthases subsequently convert PGH<sub>2</sub> into potent lipid-signaling molecules that are tasked with regulating “housekeeping” functions required for normal physiological activities and that are also associated with a number of pathologies, including inflammation and cancer (3, 4). Both COX-1 and COX-2 are the pharmacological targets of aspirin and other nonsteroidal anti-inflammatory drugs, which are utilized for the treatment of pain and inflammation (5). COX-2 can also be selectively inhibited by the recently developed coxibs: diaryl-heterocycle-based compounds that include celecoxib, rofecoxib, valdecoxib, and etoricoxib (6).

The catalytic mechanism and molecular basis underlying the conversion of AA to PGH<sub>2</sub> by COX-1 and COX-2 has been established utilizing structural and functional studies carried out over the past 20+ years (reviewed in Refs. 7 and 8). The COX enzymes are membrane-associated, heme-containing homodimers that contain spatially distinct but functionally linked cyclooxygenase and peroxidase active sites. In its productive conformation, AA is oriented in the cyclooxygenase channel with the carboxylate group of the substrate located near Arg-120 and Tyr-355 at the opening of the channel and the  $\omega$ -end of the substrate bound in a hydrophobic groove above Ser-530 (9, 10). The productive binding of AA results in a conformation that places carbon 13 below the side chain of Tyr-385. After a preliminary catalytic turnover at the peroxidase active site, an oxy-ferryl porphyrin radical is generated, which in turn transfers an electron to Tyr-385. The resulting tyrosyl radical abstracts the 13-*proS* hydrogen to initiate cyclooxygenase catalysis. AA undergoes a bis-dioxygenation to form the intermediate PGG<sub>2</sub>. The released intermediate then binds to the peroxidase active site, where the 15-hydroperoxide group of PGG<sub>2</sub> is reduced to form PGH<sub>2</sub>. It has been recently demonstrated that both COX-1 and COX-2 oxygenate AA and other fatty acid substrates via a half-of-sites reactivity mechanism, such that at any given time, only one monomer of the homodimer is functional (11, 12).

Both COX-1 and COX-2 preferentially oxygenate AA. COX-2 has been shown to selectively utilize an extensive array of derivatives of AA as substrates, including arachidonoyl ethanolamide (anandamide; AEA) (13, 14), 2-arachidonoyl glycerol

glycerol; 2-AGE, 2-arachidonoyl glycerol ether; AEA, arachidonoyl ethanolamide; EPA, eicosapentaenoic acid;  $\mu$ , murine;  $\beta$ OG,  $\beta$ -octylglucoside; HETE-G, hydroxyeicosatetraenoic acid glyceryl ester.

(2-AG) (15, 16), and *N*-arachidonoyl glycine (17). 2-AG and AEA are widely distributed in mammalian tissues and were the first characterized endogenous ligands for the cannabinoid receptors CB<sub>1</sub> and CB<sub>2</sub> (18). COX-2 oxygenates endocannabinoid substrates using the same catalytic mechanism employed for AA, generating prostaglandin, thromboxane, and prostacyclin ethanoloamides, glycerol esters, and glycines (16, 19, 20). The ability of COX-2 to metabolize endocannabinoid substrates suggests that this isoform may be involved in the endogenous endocannabinoid signaling system. However, the exact role that these novel signaling molecules carry out, along with their biological consequences, remains to be determined (21, 22).

We report here studies designed to investigate the structural basis of endocannabinoid substrate binding to COX-2. Using Co<sup>3+</sup>-protoporphyrin IX reconstituted apoenzyme, we determined the x-ray crystal structures of wild type and R513H muCOX-2 in complex with the 2-AG isomer 1-arachidonoyl glycerol (1-AG) to 2.20 and 2.35 Å resolution, respectively, and R513H muCOX-2 in complex with AA to 2.45 Å resolution. These structures were utilized to detail the atomic interactions involved in the binding of 1-AG in the cyclooxygenase channel of muCOX-2 and aid in the functional characterization of specific residues that govern this binding.

## EXPERIMENTAL PROCEDURES

**Materials**—The COX-2 substrates AA (5Z,8Z,11Z,14Z-eicosatetraenoic acid), 2-AG (1,3-dihydroxy-2-propanyl 5Z,8Z,11Z,14Z-eicosatetraenoic acid), 1-AG (2,3-dihydroxypropyl 5Z,8Z,11Z,14Z-eicosatetraenoic acid), 2-AGe (2-[(5Z,8Z,11Z,14Z)-5,8,11,14-icosatetraen-1-yloxy]-1,3-propanediol), *N*-arachidonoyl glycine (*N*-[1-oxo-5Z,8Z,11Z,14Z-eicosatetraenyl]-glycine), AEA (*N*-(2-hydroxyethyl)-5Z,8Z,11Z,14Z-eicosatetraenamide), and S-1 methanandamide (*N*-(2-hydroxy-1S-methylethyl)-5Z,8Z,11Z,14Z-eicosatetraenamide) were purchased from Cayman Chemical Company (Ann Arbor, MI). Co<sup>3+</sup>-protoporphyrin IX was purchased from Frontier Scientific (Logan, UT). Decyl maltoside and *n*-octyl β-D-glucopyranoside (βOG) were purchased from Anatrace (Maumee, OH). The QuikChange mutagenesis kit was purchased from Stratagene (La Jolla, CA) and the Bac-to-Bac baculovirus expression kit, and associated reagents, including *Spodoptera frugiperda* 21 (Sf21) insect cells, fetal bovine serum, fungizone, penicillin-streptomycin, and sf-900 II serum-free medium, were purchased from Invitrogen. HiTrap HP Chelating and HiPrep Sephacryl S300-HR chromatography columns were purchased from Amersham Biosciences. Oligonucleotides used for site-directed mutagenesis were purchased from Integrated DNA Technologies (Coralville, IA).

**Mutagenesis**—The variants Y355F and R513H were created with the QuikChange mutagenesis kit (Stratagene) using His<sub>6</sub> N580A mouse COX-2 in pFastBac1 as a template (10) and the following primers (note that the site of mutation is marked in bold and underlined; forward primers are listed only): Y355F, 5'-CAACACCTGAGCGGTTTCCACTTCAAACCTCAAG-3'; and R513H, 5'-GCTGGTGGAAAAACCTCATCCAGATGCTATCTTTGGGG-3'. Each mutant construct was verified by DNA sequence analysis at Roswell Park Cancer Institute DNA

Sequencing Laboratory. L531A, L531F, L531P, and L531T mutants were generated as described in Ref. 10.

**Expression and Purification**—The expression and purification of His<sub>6</sub> N580A muCOX-2 and associated mutants were carried out as described in Ref. 10. Briefly, Sf21 insect cells infected with p3 virus were grown in suspension at 27 °C and harvested 72–96 h post-infection in conjunction with a drop in cell viability to below 80%. Harvested cell pellet was resuspended in 50 mM Tris, pH 8.0, 300 mM NaCl, 10 mM imidazole, and 1 mM 2-mercaptoethanol, ruptured using a microfluidizer (Microfluidics, Newton, MA), and solubilized with decyl maltoside. Following centrifugation at 40,000 rpm at 4 °C for 1 h, the supernatant was loaded on a 5-ml HiTrap Chelating HP column and washed with buffer A (50 mM Tris, pH 8.0, 300 mM NaCl, 20 mM imidazole, 1 mM 2-mercaptoethanol, and 0.5% (w/v) decyl maltoside). The column was then washed with buffer B (buffer A containing a final concentration of 60 mM imidazole), protein eluted with buffer C (buffer A containing 200 mM imidazole), followed by pooling and dialysis overnight at 4 °C against 50 mM Tris, pH 8.0, 300 mM NaCl, and 0.53% (w/v) βOG for utilization in functional studies. For crystallization, the immobilized metal affinity purified His<sub>6</sub> N580A muCOX-2 was trypsin digested for 20–90 min at 25 °C with a 30:1 ratio COX-2:trypsin (23), followed by termination of the reaction via the addition of 2 mM phenylmethylsulfonyl fluoride. The trypsinized His<sub>6</sub> N580A muCOX-2 was then subjected to size exclusion chromatography utilizing a HiPrep 16/60 Sephacryl S-300 HR column equilibrated in 25 mM Tris, pH 8.0, 150 mM NaCl, and 0.53% (w/v) βOG. Peak fractions were pooled and concentrated to 3 mg/ml for crystallization trials.

**Cyclooxygenase and Peroxidase Assays**—For measurement of cyclooxygenase activity, the initial rate of oxygen uptake was measured at 37 °C using a YSI model 5300 biological oxygen monitor (Yellow Springs Instrument Co., Yellow Springs, OH) equipped with an oxygen electrode. Each standard assay mixture contained 3 ml of 100 mM Tris, pH 8.0, 1 mM phenol, 5 μM hematin, and 2–200 μM substrate. The reactions were initiated by the addition of 3–10 μg of protein in a volume of 20 μl. Initial reaction velocity data were obtained from the linear portion of oxygen uptake curves using DASyLab 10.0 software for Windows (DASYTEC USA, Bedford, NH). For the determination of *K<sub>m</sub>*, *V<sub>max</sub>*, and *k<sub>cat</sub>* values, oxygen uptake was measured, and the data were fit using nonlinear regression to the Michaelis-Menten equation with GraphPad Prism 5.0 for Windows (GraphPad Software, San Diego, CA). In preparation for the use of 1-AG, 2-AG, and 2-AGe in the cyclooxygenase assay, the 10 mg/ml stock of each endocannabinoid substrate in acetonitrile was evaporated under a stream of nitrogen gas and resuspended in ethanol for dilution into the assay buffer and use at the appropriate concentrations. Cyclooxygenase assays utilizing 2-AG were carefully timed given the substrate's short half-life under biological buffer and aqueous conditions and its ability to structurally rearrange to 1-AG via acyl migration (24). Peroxidase activity was measured spectrophotometrically at 25 °C. The reaction mixture in the cuvette contained 100 mM Tris, pH 8.0, 100 μM *N,N,N',N'*-tetramethylphenylenediamine, 1.7 μM hematin, and up to 100 μg of protein. The reactions were initi-

**TABLE 1**  
Data collection and refinement statistics

Crystallographic parameter	COX-2:1AG	R513H:AA	R513H:1AG
Space group	I222	I222	I222
No. in asymmetric unit	2	2	2
<b>Unit cell length (Å)</b>			
a	118.96	121.15	121.31
b	131.77	132.05	131.75
c	179.86	180.76	180.02
$\alpha = \beta = \gamma$ (°)	90°	90°	90°
Wavelength (Å)	0.9777	0.9780	0.9780
Resolution (Å)	20.0–2.20	20.0–2.45	20.0–2.35
Highest resolution shell (Å)	2.32–2.20	2.58–2.45	2.48–2.35
$R_{\text{merge}}^{a,b}$	8.6 (41.7)	9.9 (53.6)	12.4 (57.6)
$R_{\text{pim}}$	4.5 (24.5)	5.0 (26.8)	6.1 (28.6)
Total observations	320088 (35997)	259257 (37347)	294919 (43041)
Total unique <sup>c</sup>	71165 (9915)	53369 (7699)	59835 (8694)
$I/\sigma(I)$	11.4 (2.8)	11.8 (2.7)	10.4 (2.7)
Completeness (%)	99.2 (95.9)	99.8 (100.0)	99.6 (100.0)
Multiplicity	4.5 (3.6)	4.9 (4.9)	4.9 (5.0)
Wilson B factor (Å <sup>2</sup> )	30.3	43.5	33.2
Number of atoms in refinement	10254	9793	9949
$R_{\text{work}}^d$	0.168 (0.231)	0.163 (0.225)	0.162 (0.205)
$R_{\text{free}}^e$	0.215 (0.298)	0.219 (0.293)	0.214 (0.249)
<b>Average B factor</b>			
Protein (Å <sup>2</sup> )	25.3	30.3	21.5
Solvent (Å <sup>2</sup> )	18.3	21.2	17.3
Substrate (Å <sup>2</sup> )			
Monomer A (Å <sup>2</sup> )	49.9	42.8	55.0
Monomer B (Å <sup>2</sup> )	46.0	49.4	57.0
Mean positional error (Å) <sup>c</sup>	0.280	0.306	0.293
RMSD in bond length (Å)	0.008	0.013	0.013
RMSD in bond angle (°)	1.134	1.663	1.686

<sup>a</sup> The values in parentheses represent the values in the outermost resolution shell.

<sup>b</sup>  $R_{\text{merge}}$  and  $R_{\text{pim}}$  are as defined in Ref. 45.

<sup>c</sup> Represents reflections with  $F > 0 \sigma F$ , which were used in the refinement.

<sup>d</sup> 5.0% of the total reflections were used to generate the test set.

<sup>e</sup> Coordinate error as calculated by Luzatti plot.

ated by adding 100  $\mu\text{l}$  of 300  $\mu\text{M}$   $\text{H}_2\text{O}_2$ , and the oxidation of  $N,N,N',N'$ -tetramethylphenylenediamine was monitored at 610 nm over time.

**Crystallization and Data Collection**—For crystallization, purified apo His<sub>6</sub> N580A muCOX-2 or His<sub>6</sub> R513H/N580A muCOX-2 was reconstituted with a 2-fold molar excess of  $\text{Co}^{3+}$ -protoporphyrin IX and dialyzed overnight at 4 °C against 20 mM Tris, pH 8.0, 100 mM NaCl, 0.6% (w/v)  $\beta\text{OG}$  (10). A 10-fold molar excess of AA, 1-AG, or 2-AG was added to the reconstituted protein depending on the complex being studied. All of the crystals were grown using the sitting drop vapor diffusion technique by mixing 3  $\mu\text{l}$  of protein solution with 3  $\mu\text{l}$  of 23–34% polyacrylic acid 5100, 100 mM HEPES, pH 7.5, 20 mM  $\text{MgCl}_2$ , and 0.6% (w/v)  $\beta\text{OG}$ , and equilibrating over reservoir solutions containing 23–34% polyacrylic acid 5100, 100 mM HEPES, pH 7.5, and 20 mM  $\text{MgCl}_2$ . Plate-like crystals were observed within 1 week in crystallization drops incubated at 23 °C. The data were collected on beamline A1 at the Cornell High Energy Synchrotron Source (Ithaca, NY) using an Area Detector Systems CCD Quantum-210 detector. In preparation for synchrotron data collection, the crystals were cryoprotected by transfer to a solution consisting of 30% polyacrylic acid 5100, 100 mM HEPES, pH 7.5, 20 mM  $\text{MgCl}_2$ , 0.6% (w/v)  $\beta\text{OG}$ , supplemented with 10% ethylene glycol. The data sets were integrated and scaled using MOSFLM and SCALA respectively, in the CCP4 suite of programs (25). Details of the data collection statistics are summarized in Table 1.

**Structure Solution and Refinement**—The reduction of model bias during structure solution and refinement was minimized using the protocols outlined in Ref. 10. Briefly, initial phases for the muCOX-2:1AG, R513H:AA, and R513H:1AG structures were determined using PHASER (26) in conjunction with a truncated search model of muCOX-2 derived from the Protein Data Bank entry 1CVU that had residues 33–144, 320–325, 344–391, and 500–553, along with all associated ligands removed prior to molecular replacement calculations. Phases from the molecular replacement solution were then used as input to ARP/wARP (27) utilizing the “automated model building starting from experimental phases” option. ARP/wARP built most of the deleted portions of the models. Iterative cycles of manual model building and refinement, using COOT (28) and REFMAC5 (29), were then carried out to fit the remaining residues and to add waters, substrate, sugar moieties, and other ligand molecules. Minimized coordinates and stereochemical dictionaries for 1-AG and 2-AG were generated using Molecular Operating Environment (Chemical Computing Group, Montreal, Canada) and the PRODRG server (30), respectively translation libration screw (TLS) refinement (31), utilizing the TLSMD web server (32, 33), was carried out during the final rounds of refinement. Final refinement statistics for each complex are summarized in Table 1.

2-AG readily undergoes acyl migration to 1-AG in biological buffers (24). We first modeled 2-AG into the cyclooxygenase channel of monomer A and monomer B because it was used as the substrate for crystallization of muCOX-2:1AG. Cycles of

REFMAC5 refinement were carried out, followed by the calculation of  $2F_o - F_c$  and  $F_o - F_c$  electron density maps. The maps clearly showed that the glycerol moiety of 2-AG had rearranged to 1-AG during crystallization, given the location of negative and positive electron density peaks (supplemental Fig. S1).

**Structural Analysis**—van der Waals and hydrogen bond interactions were calculated using the program COOT. The upper limit on distance for consideration as a Van der Waals contact is 4.0 Å. Superposition of coordinates between structures was done using the program LSQAB within the CCP4 suite of programs and the coordinates for all C $\alpha$  atoms unless otherwise stated. Simulated annealing omit maps were calculated using CNS (34). Model validation was carried out using MOLPROBITY (35). The figures were created using CCP4MG (36). The coordinates and structure factors for Co<sup>3+</sup>-protoporphyrin IX reconstituted His<sub>6</sub> N580A muCOX-2 in complex with 1-AG as well as for R513H muCOX-2 in complex with AA and 1AG have been deposited in the Protein Data Bank (Protein Data Bank codes 3MDL, 3OLT, and 3OLU, respectively).

## RESULTS

**Structural Elucidation of Endocannabinoid Substrate in Complex with Murine COX-2**—We generated a stable complex of endocannabinoid substrate bound in the cyclooxygenase channel of muCOX-2 for crystallographic studies by reconstituting purified apo enzyme with Co<sup>3+</sup>-protoporphyrin IX prior to the addition of 2-AG (37). The structure was subsequently elucidated to a resolution of 2.2 Å using synchrotron radiation. There are two monomers in the crystallographic asymmetric unit (termed monomers A and B for comparison purposes) that form the canonical dimer observed for other structures of muCOX-2 in complex with fatty acid substrates (10). The calculated root mean square deviation between monomers A and B is 0.189 Å (for 551 C $\alpha$  atom pairs), indicating that there are no significant structural differences between these monomers. Furthermore, there are no significant conformational differences between monomers when either fatty acid or endocannabinoid substrate is bound in the cyclooxygenase channel (data not shown). Clear electron density was visible for endocannabinoid substrate in both monomers of the cyclooxygenase channel (Fig. 1). However, initial modeling of 2-AG into the electron density indicated that the substrate had undergone acyl migration to 1-AG during the crystallization process (see “Experimental Procedures”) (24). Hence, the crystal structure reported here represents a complex between muCOX-2 and 1-AG (muCOX-2:1AG).

In general, 1-AG exhibits a similar, global conformation within the cyclooxygenase channel of each monomer of the muCOX-2:1AG crystal structure. In both instances, the endocannabinoid substrate binds with its glycerol moiety located near Arg-120 and Tyr-355 at the opening of the cyclooxygenase channel and its  $\omega$ -end inserted into the hydrophobic groove above Ser-530 (Fig. 1). However, there are also subtle, but significant differences in the conformations of 1-AG in each monomer. Specifically, the  $\omega$ -end of 1-AG bound to monomer A does not fully insert into the hydrophobic groove, resulting in the misalignment of carbon 13 for hydrogen abstraction (Figs. 1 and 2). Conversely, the

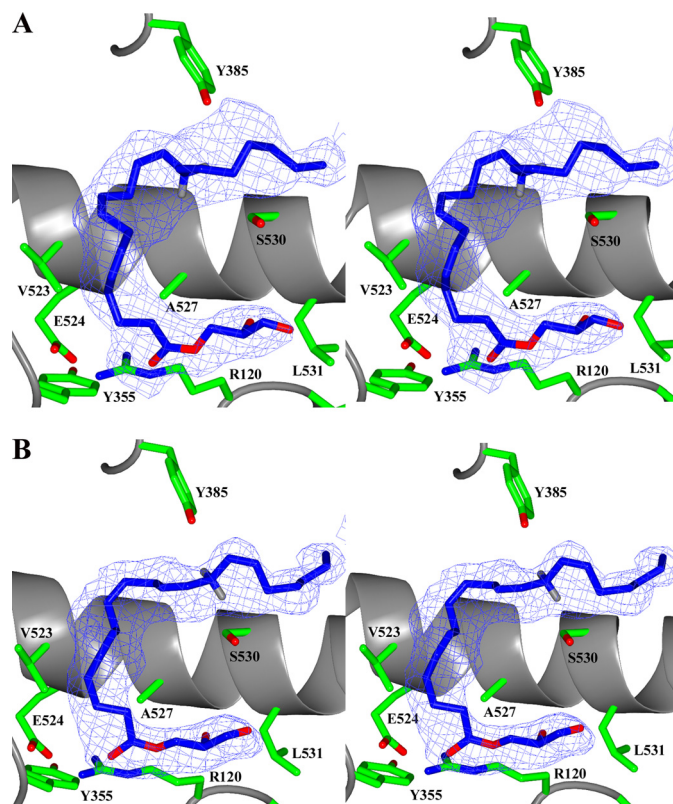


**FIGURE 1. 1-AG bound in the cyclooxygenase channel of the muCOX-2:1AG crystal structure.** Shown are stereo views of 1-AG bound in the cyclooxygenase channel in a “nonoptimal” conformation in monomer A (A) and a “productive” conformation in monomer B (B).  $F_o - F_c$  simulated annealing omit map density, contoured at  $5\sigma$ , is shown with the final refined models of 1-AG (dark blue carbon and red oxygen atoms). Hydrogen atoms have been modeled onto carbon 13 of 1-AG. The 13-*proS* hydrogen of 1-AG bound in monomer B lies 3.3 Å below the phenolic oxygen of Tyr-385.

$\omega$ -end of 1-AG bound in monomer B binds deep into the hydrophobic groove so that the terminal carbon abuts with the side chain of Ile-377, resulting in the optimal alignment of carbon 13 below Tyr-385 for hydrogen abstraction and subsequent catalysis. The magnitude of the shift in the placement of the  $\omega$ -end is reflected in the calculated root mean square deviation of 2.18 Å between the two 1-AG conformations, with the major differences arising between the positions for carbons 8–20 (supplemental Table S1). Thus, crystal structure analysis indicates that within the biological dimer, 1-AG binds in a nonproductive conformation in monomer A and in a productive conformation in monomer B, analogous to that observed for AA and EPA in the muCOX-2:AA and muCOX-2:EPA crystal structures (Fig. 2) (10) and consistent with the proposed model for half-of-sites activity for cyclooxygenase enzymes (12).

In the productive conformation, 1-AG binds with its 2,3-dihydroxypropyl moiety located in the space above the side chain of Arg-120 made available by the movement of the side chain of Leu-531 into a different rotamer conformation (Figs. 1 and 2). The movement of the Leu-531 side chain is identical to that observed when AA binds in its nonproductive conformation in the muCOX-2:AA crystal structure (10, 38). This is the only difference between the positions of the side chains of the residues that line the cyclooxygenase channel. 1-AG makes a

## Endocannabinoid Substrate Binding to COX-2

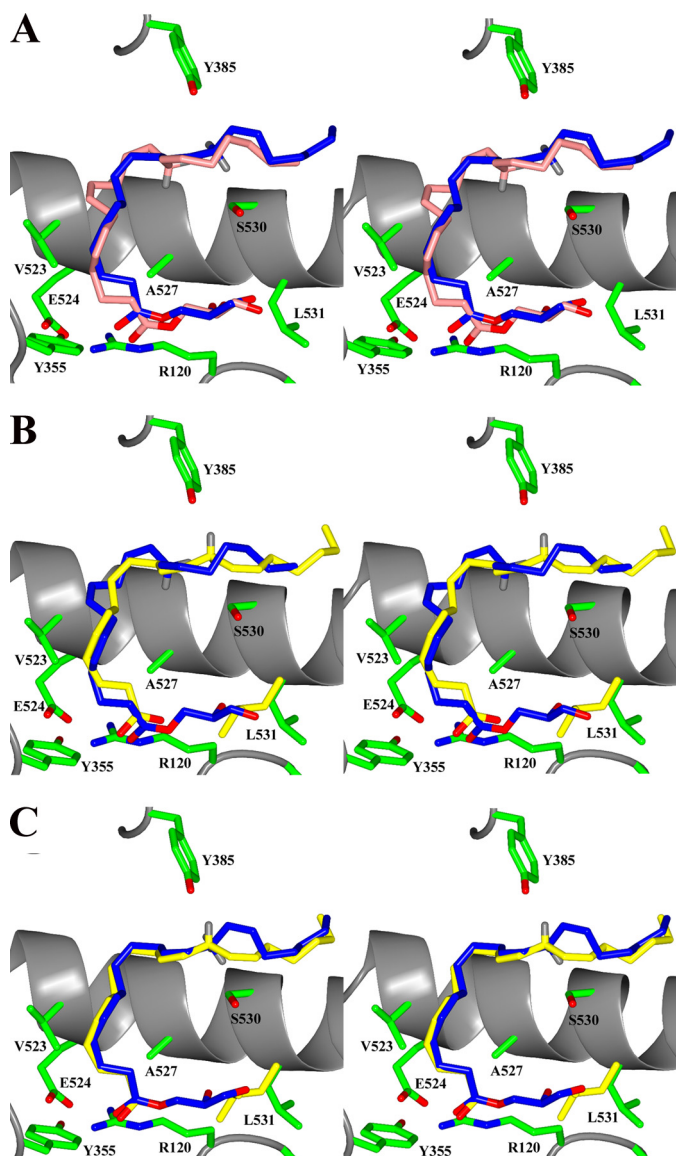


**FIGURE 2. Comparison of the binding modes of 1-AG and AA in the cyclooxygenase channel.** *A*, stereo view of 1-AG bound in a “productive” conformation in monomer B (dark blue) versus 1-AG bound in a nonoptimal conformation in monomer A (pink) of the muCOX-2:1AG crystal structure. The  $\omega$ -end of 1-AG does not protrude completely into the hydrophobic groove above Ser-530 in monomer A, resulting in the misalignment of carbon 13. *B* and *C*, stereo views of the superposition of the productive conformation of AA (yellow) from monomer B of the muCOX-2:AA crystal structure (10) with the conformation of 1-AG from monomer A (*B*) and monomer B (*C*) of the muCOX-2:1AG crystal structure. Cyclooxygenase channel residues in the muCOX-2:1AG crystal structure are shown in green and labeled accordingly, whereas the position of Leu-531 in monomer B of the muCOX-2:AA crystal structure is shown in yellow. Nitrogen atoms are shown in blue, and oxygen atoms are in red.

total of 62 contacts with 18 residues lining the cyclooxygenase channel (supplemental Table S2). The 2,3-dihydroxypropyl moiety of 1-AG is not stabilized by ionic or hydrogen bonding interactions with the polar side chain atoms of Arg-120, Arg-513, or Glu-524 at the opening of the channel as previously hypothesized (13, 15, 17). The central carbons and  $\omega$ -end of 1-AG bind similar to that of AA bound productively within the cyclooxygenase channel (Fig. 2). The calculated root mean square deviation for the positions of the 22 equivalent atoms between 1-AG and AA is 0.7 Å (supplemental Table S3).

*Functional Analysis of Residues at the Opening of the Cyclooxygenase Channel Involved in Endocannabinoid Catalysis*—To compliment our structural observations, we determined the kinetic parameters associated with the oxygenation of endocannabinoid substrates by wild type and mutant constructs of COX-2. The endocannabinoids 2-AG, 1-AG, 2-AGe, AEA, *N*-arachidonoyl glycine, and S-1 methanandamide were oxygenated at varying rates, when compared with the rate of oxygenation of AA (supplemental Figs. S2 and S3). Both 2-AG and 1-AG were preferred over the other endocannabinoid substrates, exhibiting oxygenation rates of 88 and 73%, respectively, compared with AA, and their calculated  $K_m$  values were comparable with those reported previously for AA and 2-AG (Table 2) (16). The kinetic constants associated with 2-AGe oxygenation have not previously been characterized. 2-AGe is oxygenated by muCOX-2 at 46% the rate of AA and 62% the rate of 2-AG, with  $k_{cat}$  and  $K_m$  values calculated to be  $12.3 \pm 0.3 \text{ s}^{-1}$  and  $6.3 \pm 0.5 \mu\text{M}$ , respectively. In general, we observed oxygenation rates for AEA, *N*-arachidonoyl glycine, and S-1 methanandamide that were comparable with those reported previously utilizing muCOX-2 and human COX-2 constructs (13, 14, 17). Given that the 2,3-dihydroxypropyl group of 1-AG: (*a*) binds in a different location within the cyclooxygenase channel in our crystal structure than that previously hypothesized for endocannabinoid substrates and (*b*) does not form extensive hydrophilic contacts with residues near the opening of the cyclooxygenase channel, we further evaluated the role that Tyr-355, Arg-513, and Leu-531 play in the binding and oxygenation of these substrates.

*Tyrosine 355*—Tyr-355 is located opposite Arg-120 at the base of the cyclooxygenase channel, where it contributes to the formation of an “aperture” via water-mediated hydrogen bonding interactions with the side chains of His-90, Arg-513, and Glu-524 (7). The phenolic hydroxyl group of Tyr-355 has been shown to form a hydrogen bond with the carboxylate group of fatty acid substrates in their productive conformations (9, 10, 39, 40). Mutation of Tyr-355 to phenylalanine results in an enzyme with a ~50% decrease in the cyclooxygenase activity and 2.5-fold increase in  $K_m$  relative to wild type enzyme, when AA is utilized as the substrate (Table 2) (23, 41). The observed reduction in cyclooxygenase activity and increase in  $K_m$  are likely due to an increase in mobility for the fatty acid substrate in the cyclooxygenase channel caused by: (*a*) the loss of the hydrogen bond with the carboxylate group and (*b*) the lack of a required interaction of the carboxylate of AA with the side chain of Arg-120 (10, 42).

In contrast to that observed when AA is utilized as a substrate, Y355F muCOX-2 exhibits increased oxygenation rates for 2-AG and 1-AG compared with the oxygenation of these substrates by wild type enzyme (Fig. 3). Moreover, there is a 3.1-fold decrease in  $K_m$  for 2-AG, suggesting that 2-AG binds in a more optimal conformation within the cyclooxygenase channel of Y355F muCOX-2 for catalysis (Table 2). In the muCOX-2:1-AG crystal structure, the phenolic hydroxyl group of Tyr-355 makes a single contact with the endocannabinoid substrate in its productive conformation: a strong hydrogen bond to the carboxylate oxygen of 1-AG (2.89 Å; supplemental Table S2). The increase in oxygenation observed for 2-AG and 1-AG, and

TABLE 2

## Oxygenation of AA, 1-AG, and 2-AG by wild type and mutant constructs of muCOX-2

Oxygen consumption was measured using an oxygen electrode as described under "Experimental Procedures."  $k_{\text{cat}}$  and  $K_m$  values were derived from triplicate measurements, utilizing 5  $\mu\text{g}$  of protein in the electrode chamber.  $E$ , efficiency, defined as  $k_{\text{cat}}/K_m$ ; ND, not determined.

Construct	AA			2-AG			1-AG		
	$k_{\text{cat}}$	$K_m$	$E$	$k_{\text{cat}}$	$K_m$	$E$	$k_{\text{cat}}$	$K_m$	$E$
	$s^{-1}$	$\mu\text{M}$		$s^{-1}$	$\mu\text{M}$		$s^{-1}$	$\mu\text{M}$	
Wild-type	27.0 $\pm$ 0.4	5.1 $\pm$ 0.3	5.2	23.7 $\pm$ 1.7	8.5 $\pm$ 1.6	2.8	19.7 $\pm$ 1.0	7.3 $\pm$ 1.1	2.7
Y355F	15.0 $\pm$ 0.3	12.3 $\pm$ 0.8	1.2	23.8 $\pm$ 0.7	2.7 $\pm$ 0.3	8.8	ND	ND	ND
R513H	28.7 $\pm$ 0.5	11.0 $\pm$ 0.6	2.6	19.7 $\pm$ 0.9	7.2 $\pm$ 1.0	2.7	19.1 $\pm$ 0.8	9.1 $\pm$ 1.1	2.1
L531A <sup>a</sup>	13.9 $\pm$ 0.3	3.7 $\pm$ 0.3	3.8	14.9 $\pm$ 0.4	4.4 $\pm$ 0.4	3.4	ND	ND	ND
L531F	23.3 $\pm$ 0.4	14.9 $\pm$ 0.8	1.6	18.9 $\pm$ 0.6	7.3 $\pm$ 0.8	2.6	19.5 $\pm$ 0.6	7.1 $\pm$ 0.6	2.7
L531P	14.9 $\pm$ 0.3	2.9 $\pm$ 0.3	5.1	16.3 $\pm$ 0.9	8.2 $\pm$ 1.2	2.0	ND	ND	ND

<sup>a</sup> Kinetic parameters for the oxygenation of AA by wild-type enzyme, as well as L531A and L531P mutant constructs, are from Ref. 10.

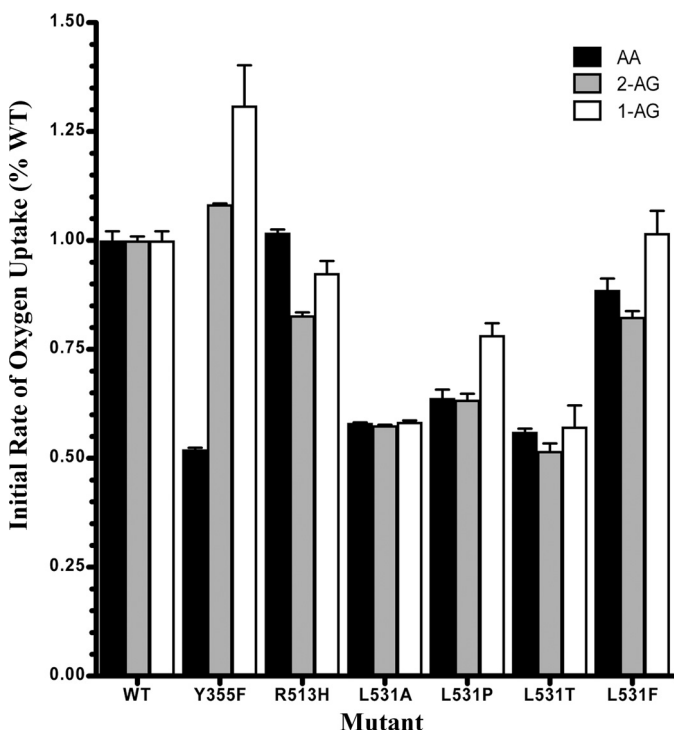


FIGURE 3. Oxygenation of AA, 2-AG, and 1-AG by wild type and mutant constructs of muCOX-2. Shown is a bar graph depicting the initial rate of oxygen uptake by wild type and mutant constructs of muCOX-2 utilizing AA, 2-AG, and 1-AG as substrates. Each mutant is normalized to the initial rate of oxygen uptake for each of the three substrates with wild type enzyme. Normalized values represent duplicate measurements carried out at substrate concentrations of 25  $\mu\text{M}$  and using 5  $\mu\text{g}$  of enzyme in the electrode chamber, with error bars representing the standard deviation between measurements.

the decrease in  $K_m$  for 2-AG compared with wild type enzyme can be rationalized by the lack of participation of the phenolic hydroxyl of Tyr-355 in the water-mediated hydrogen-bonding network at the base of the cyclooxygenase channel. As a result, the 2,3-dihydroxypropyl group of 1-AG has greater mobility to realign into a more optimal binding conformation for catalysis. The observed increase in the proportion of prostaglandin glycerol ester to hydroxyeicosatetraenoic acid glycerol ester (HETE-G) product generated for the Y355F muCOX-2 mutant compared with wild type enzyme lends further credence to this idea (15).

**Arginine 513**—Arg-513 (histidine in COX-1) along with Val-434 and Val-523 (both isoleucine residues in COX-1) are the only differences between the first and second shell of residues that constitute the cyclooxygenase channel. These changes

generate a side pocket, exclusive to COX-2, that results in an increase in the overall volume of the COX-2 cyclooxygenase channel by  $\sim 20\%$  (7). The presence of Arg-513 at the center of this side pocket has been exploited in the design of the diaryl-heterocycle class of COX-2-selective inhibitors (reviewed in Ref. 5). The side chain of Arg-513 is located  $\sim 7.0$  Å away from AA bound in its productive conformation within the cyclooxygenase channel of COX-2 and hence does not contact or influence binding or catalysis of fatty acid substrates (10). In addition, the side chain of Arg-513 participates in the water-mediated hydrogen bond network that serves to constrict the opening of the cyclooxygenase channel upon substrate binding.

In the muCOX-2:1AG crystal structure, the COX-2-selective side pocket is devoid of any substrate atoms, and the side chain of Arg-513 is located  $\sim 8.4$  Å away from 1-AG. This observation was somewhat of a surprise given previous studies implicating Arg-513 as an isoform-specific molecular determinant governing endocannabinoid binding and catalysis by COX-2 (13, 15, 17). Given the discrepancy between the previous functional studies and our crystal structure analysis, we generated the R513H muCOX-2 construct and carried out kinetic analyses utilizing AA, 2-AG, and 1-AG as substrates. Consistent with previous observations, R513H muCOX-2 oxygenated AA at virtually the same rate as wild type enzyme, albeit with a 2.2-fold increase in  $K_m$  (Table 2 and Fig. 3) (13, 15, 17). In contrast, R513H muCOX-2 efficiently oxygenated both 2-AG and 1-AG when compared with the oxygenation of these substrates by wild type enzyme, with no significant change in  $K_m$  (Table 2). These results are in line with prostaglandin glycerol ester and HETE-G product analyses, which showed no change in the ratio of the products generated from 2-AG by either wild type or R513H muCOX-2 constructs (15).

**Leucine 531**—Leu-531 is located above the side chain of Arg-120 near the opening of the cyclooxygenase channel. The side chain of Leu-531 does not interact with fatty acid substrate when it is bound productively in the cyclooxygenase channel of ovine COX-1 or muCOX-2 (9, 10, 39, 40). Instead, it forms hydrophobic contacts with the side chain of Arg-120. It has been postulated that these interactions provide a stabilizing effect for the side chain of Arg-120 such that high affinity binding is maintained in ovine COX-1 (43). Conversely, mutating the side chain of Leu-531 to Ala, Phe, Pro, or Thr in muCOX-2 does not result in a decrease in substrate binding or a significant loss of cyclooxygenase activity caused by the lack of a require-

## Endocannabinoid Substrate Binding to COX-2

ment for the substrate to interact with the side chain of Arg-120 for proper catalysis (Table 2) (10, 42).

When AA and EPA bind in a nonproductive conformation to muCOX-2, the side chain of Leu-531 exhibits an alternate rotamer conformation that allows for the accommodation of the  $\omega$ -end of the substrate above the side chain of Arg-120 near the opening of the channel (10). We speculated that rather than playing a role in high affinity binding of substrate, the mobility of Leu-531 increases the volume of and contributes to the flexibility at the opening of the cyclooxygenase channel that in turn influences the ability of certain substrates to bind preferentially to COX-2 (10). Accordingly, the side chain of Leu-531 exhibits this rotamer conformation in both monomer A and monomer B of the muCOX-2:1AG crystal structure, creating space for the 2,3-dihydroxypropyl moiety to bind into (Fig. 2).

To investigate the role that the flexibility of the Leu-531 side chain had on the oxygenation of endocannabinoid substrates, we generated L531A, L531F, L531P, and L531T mutant constructs (10). All four constructs retained significant levels of cyclooxygenase activity, compared with wild type enzyme, when either AA, 2-AG, or 1-AG were utilized as substrates (Fig. 3). The L531A mutant construct exhibited similar  $K_m$  values for AA and 2-AG, although both were 1.4–1.9-fold lower than that observed with wild type enzyme (Table 2). The L531P construct had a similar  $K_m$  value for 2-AG as wild type enzyme but a 2.8-fold lower  $K_m$  value when AA was utilized as the substrate (Table 2). The L531F mutant construct maintained the highest amount of cyclooxygenase activity of all the mutants tested. Interestingly, the L531F mutant construct exhibits similar  $K_m$  values for 2-AG and 1-AG, compared with wild type enzyme, but a 2-fold higher  $K_m$  value when AA is utilized as the substrate (Table 2). Taken together, Leu-531 mutations do not affect the binding of endocannabinoid substrate in the cyclooxygenase channel and only moderately affect the oxygenation of these substrates by COX-2. These results also agree with previous studies showing that a reduction in the size of the hydrophobic side chain of Leu-531 had a less profound effect on the oxygenation of the endocannabinoids 2-AG and AEA, compared with the oxygenation of AA by these mutants (13, 15).

**The Structural Consequences Associated with Substrate Binding to R513H COX-2**—To further probe the structural consequences that the R513H substitution has on the binding of fatty acid and endocannabinoid substrates in the cyclooxygenase channel of muCOX-2, we determined the crystal structures of Co<sup>3+</sup>-protoporphyrin IX reconstituted R513H muCOX-2 in complex with AA and 1-AG (denoted R513H:AA and R513H:1AG, respectively). Both the R513H:AA and R513H:1AG crystal structures contain a dimer within their asymmetric units. The major structural consequence of the R513H mutation, common to both the R513H:AA and R513H:1AG crystal structures, is the loss of an ionic interaction and hydrogen bond between the side chains of Arg-120 and Glu-524 and the loss of the interactions between the side chains of Asn-87 and Arg-513. As a consequence, only one of the seven ordered waters observed in the muCOX-2:AA and muCOX-2:1AG crystal structures remain in the R513H:AA and R513H:1AG crystal structures (supplemental Fig. S4). The loss of the interactions between the side chain of Asn-87 and Arg-513 results in the

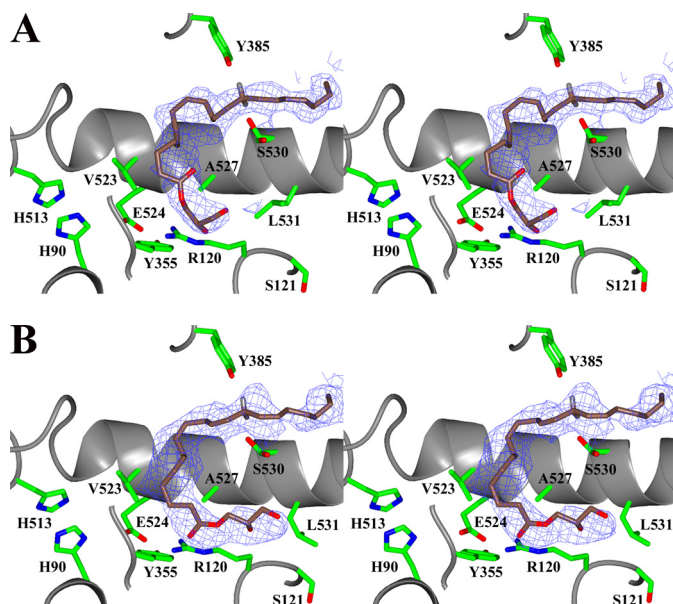


**FIGURE 4. 1-AG bound in the cyclooxygenase channel of the R513H:1AG crystal structure.** Stereo view of 1-AG bound in the cyclooxygenase channel in monomer A (A) and monomer B (B).  $2F_o - F_c$  simulated annealing omit map density, contoured at  $5\sigma$ , is shown with the final refined models of 1-AG (copper carbon and red oxygen atoms). Hydrogen atoms have been modeled onto carbon 13 of 1-AG. Selected residues at the opening and lining the cyclooxygenase channel are shown in green and labeled accordingly.

decoupling of helix B of the membrane-binding domain from the base of the catalytic domain.

In the R513H:AA crystal structure, AA is bound in a nonproductive conformation in monomer A and a productive conformation in monomer B, nearly identical to that observed in the muCOX-2:AA crystal structure (supplemental Figs. S5 and S6) (10) and in agreement with our kinetic analyses (Table 2). In the observed productive conformation, carbon 13 is aligned properly below the phenolic oxygen of Tyr-385 for catalysis. However, there is a loss of eight contacts between AA and the residues lining the cyclooxygenase channel, compared with the equivalent contacts observed for the productive binding of AA in the muCOX-2:AA crystal structure (supplemental Table S4) (10). Among the contacts lost is the hydrogen bond between the phenolic oxygen of Tyr-355 and the carboxylate of AA. As a result, the carboxylate portion of the substrate is not tethered to the mouth of the cyclooxygenase channel and thus can become more mobile in the active site. Taken together, these structural observations coincide with the 2.2-fold increase in  $K_m$  observed for the R513H mutant construct when AA is utilized as the substrate (Table 2).

In each monomer of the R513H:1AG crystal structure, the  $\omega$ -end of 1-AG binds deep in the hydrophobic groove above Ser-530, and carbon 13 lies below Tyr-385 poised for catalysis, consistent with productive binding of substrate in the cyclooxygenase channel. However, the 2,3-dihydroxypropyl moiety is bound in a different conformation in each monomer (Fig. 4). The overall conformation of 1-AG observed in monomer B of the R513H:1AG crystal structure is nearly identical to that seen for 1-AG in monomer B of the muCOX-2:1AG crystal structure, and the contacts made between 1-AG and the residues lining the cyclooxygenase channel are virtually conserved

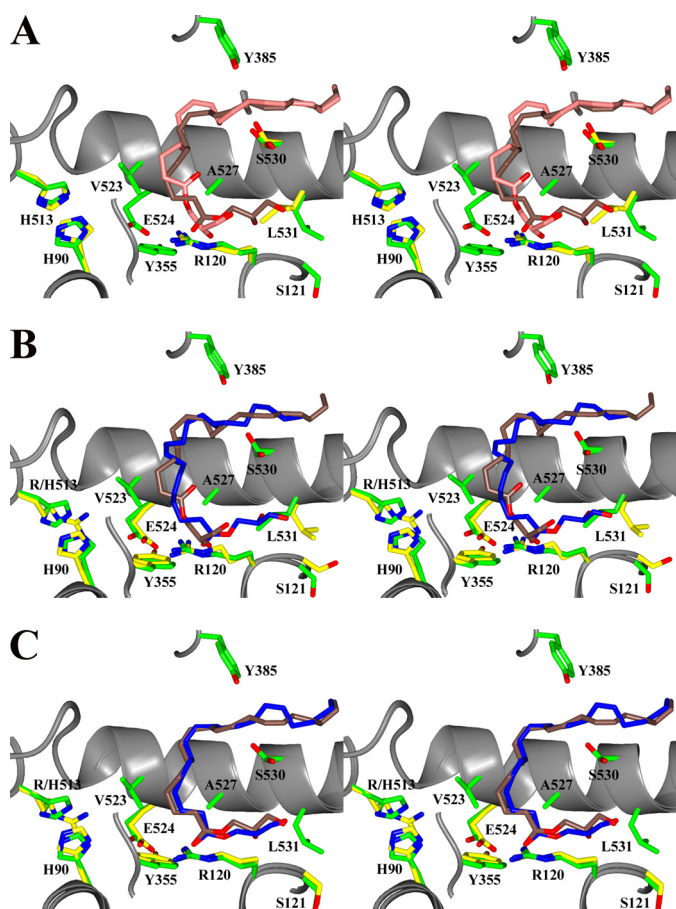


**FIGURE 5. Comparison of the binding modes of 1-AG in the cyclooxygenase channels of the muCOX-2:1AG and R513H:1AG crystal structures.** A, stereo view of 1-AG bound in the cyclooxygenase channel of monomer A (pink) and monomer B (copper) in the R513H:1AG crystal structure. The 2,3-dihydroxypropyl moiety and carbons 1–13 of 1-AG in monomer A are compressed in the lower portion of the cyclooxygenase channel. B and C, stereo views of the superposition of the productive conformation of 1-AG from monomer B of the muCOX-2:1AG crystal structure (blue) with the conformation of 1-AG from monomer A (B) and monomer B (C) of the R513H:1AG crystal structure. Cyclooxygenase channel residues in the muCOX-2:1AG crystal structure are shown in yellow, whereas the equivalent residues from the R513H:1AG crystal structure are shown in green. In both cases, nitrogen atoms are shown in blue, and oxygen atoms are shown in red.

(supplemental Table S5). The 2,3-dihydroxypropyl moiety is still located near Arg-120 in the space generated by the movement of the side chain of Leu-531 into a different rotamer conformation. As a consequence of the loosened aperture, the 2,3-dihydroxypropyl group repositions such that it now makes a hydrophilic contact with the side chain of Arg-120 instead of a long hydrogen bond with the carbonyl oxygen of Ala-527. In monomer A, 1-AG binds with the 2,3-dihydroxypropyl moiety positioned away from the side chain of Leu-531, which now exhibits a rotamer conformation equivalent to that observed when AA is bound productively in the cyclooxygenase channel (Fig. 5). In this conformation, 1-AG makes an additional hydrophilic contact with the Ne atom of Arg-120 (supplemental Table S6). As a result, carbons 1–13 of 1-AG are compressed between the opening and the apex of the cyclooxygenase channel, similar to that observed for EPA bound in the cyclooxygenase channel of COX-1 (39) and docosahexaenoic acid bound in the cyclooxygenase channel of COX-2 (10). In this com-

pressed conformation, 1-AG makes an additional 15 contacts with the residues lining the cyclooxygenase channel (supplemental Table S6).

## DISCUSSION

We observe electron density in the cyclooxygenase channel of each monomer of the muCOX-2:1-AG crystal structure consistent with the binding of 1-AG in the channel. However, the conformation of 1-AG in each monomer is different. The observation of productive and nonproductive binding conformations for 1-AG is consistent with the observation of productive and nonproductive conformations of substrate in each monomer of the previously determined muCOX-2:AA and muCOX-2:EPA crystal structures (10) and with the model put forth for half-of-sites activity for cyclooxygenase (12). For AA and EPA, the nonproductive binding conformations involve the interaction of the carboxylate group of these substrates with the side chains of Tyr-385 and Ser-530 at the apex of the cyclooxygenase channel and the placement of the  $\omega$ -end near the opening of the channel. The bulky 2,3-dihydroxypropyl moiety precludes 1-AG (and presumably other endocannabinoid substrates) from binding in a similar nonproductive conformation. Instead, the  $\omega$ -end of 1-AG does not fully penetrate the hydrophobic groove above Ser-530 in monomer A. As a consequence, carbon 13 is misaligned below Tyr-385. The observed differences in nonproductive binding between the fatty acids AA and EPA and the endocannabinoid 1-AG validate CuP-induced cross-linking studies, which suggest that there are differences in the way that AA and 2-AG interact with COX-2 (12).

Surprisingly, we do not observe any interaction between 1-AG and the side chain of Arg-513, which is 8.4 Å from the nearest atom of the 2,3-dihydroxypropyl moiety. In contrast to earlier studies reporting significant decreases in the oxygenation of endocannabinoid substrates by R513H muCOX-2, we observed efficient oxygenation of 1-AG and 2-AG by the R513H mutant construct. It is not clear why there is such a discrepancy in the previously reported oxygenation rates for these endocannabinoids compared with the rates reported in this study. One possibility may be related to the relatively high substrate concentrations (200  $\mu$ M) used in the previous studies (13, 15, 17). The kinetic data presented here for R513H muCOX-2 are consistent both with the observed productive conformation of 1-AG in monomer B of the muCOX-2:1AG crystal structure and with the observation that the prostaglandin glyceryl ester and HETE-G ratios generated by wild type and R513H muCOX-2 are similar when 2-AG is utilized as the substrate (15).

The conformations observed for AA in each monomer of the R513H:AA crystal structure were nearly identical to those observed for AA binding to wild type enzyme in the muCOX-2:AA crystal structure. When AA is bound in the productive conformation in monomer B, there is a loss of eight contacts between substrate and the residues lining the cyclooxygenase channel, including the loss of the hydrogen bond between the phenolic oxygen of Tyr-355 and the carboxylate of AA. As a consequence, the carboxylate of the substrate is not tethered to the opening of the channel and thus has increased mobility.

## Endocannabinoid Substrate Binding to COX-2

This observation coincides with the observed 2.2-fold increase in  $K_m$ .

The increased flexibility observed as a result of the R513H mutation affects the way 1-AG binds in the cyclooxygenase channel as well. Although we still observe two different binding modes for 1-AG in the R513H:1AG crystal structure, the  $\omega$ -end of the endocannabinoid substrate binds in a similar manner in each monomer, deep within the hydrophobic groove above Ser-530. Although the 2,3-dihydroxypropyl moiety of 1-AG in monomer B binds in a conformation similar to that observed in the muCOX-2:1AG crystal structure, we observe a significant shift in the 2,3-dihydroxypropyl moiety of 1-AG in monomer A, away from the side chain of Leu-531. In this conformation, 1-AG is compressed within the cyclooxygenase channel, similar to that observed for EPA binding to ovine COX-1 (39) and docosahexaenoic acid binding to muCOX-2 (10). Given that carbon 13 of 1-AG is aligned below the phenolic oxygen of Tyr-385 in each monomer, we cannot rule out the possibility that each conformation potentially represents a productively bound endocannabinoid substrate. However, we speculate that the conformation observed in monomer B represents 1-AG bound to the “catalytic monomer” and the compressed conformation of 1-AG observed in monomer A represents 1-AG bound to the “allosteric monomer” (12). Additional structural and functional analyses will be required to further explore the issue.

Why are endocannabinoid substrates oxygenated more efficiently by COX-2 than COX-1? One possibility may lie in the differences observed in the sensitivity of Leu-531 to mutation in COX-1 versus COX-2 (10, 43, 44). The side chain of Leu-531 does not contact fatty acid substrate in the muCOX-2:AA and muCOX-2:EPA crystal structures. Instead, the side chain of Leu-531 is flexible, where alternate rotamer conformations are observed when AA and EPA are bound in their nonproductive and productive conformations. We speculated that the observed rotamer conformations of Leu-531 provide COX-2 with the flexibility to increase the volume at the opening of the cyclooxygenase channel, allowing for a broader spectrum of substrates to be oxygenated (10). Consistent with our hypothesis, we observe the 2,3-dihydroxypropyl moiety of 1-AG bound in the space vacated by the movement of Leu-531 in each monomer of the muCOX-2:1AG crystal structure. Binding of the ethanolamide, glycerol, or glycine moieties in this space would not have been considered in the previous models, given that the side chain of Leu-531 was fixed during molecular dynamics simulations (13, 15, 17).

Mutation of the Leu-531 side chain to Ala, Phe, Pro, or Thr had modest effects on the oxygenation of 1-AG, and 2-AG substrates. Our kinetic observations do not coincide with previous studies of L531A muCOX-2, which had less than 1% relative oxygenase activity, compared with wild type enzyme when AA was utilized as a substrate (13). However, they do coincide with observations that shortening of the Leu-531 side chain does not significantly alter the ability of these mutants to oxygenate 2-AG (15). Interestingly, the L531F mutant exhibited the highest oxygenase activity of the Leu-531 mutants tested when 1-AG and 2-AG were utilized as substrates. The phenylalanine substitution would be expected to decrease the available vol-

ume for endocannabinoid binding in the channel, assuming that there is not enough space for an alternate rotamer conformation. We saw no change in the  $K_m$  for the L531F mutation when 1-AG and 2-AG were utilized as substrates, compared with wild type enzyme. The observed  $K_m$  values for 1-AG and 2-AG oxygenation by the L531F mutant can be rationalized by the binding of the  $\omega$ -end deeply within the hydrophobic groove above Ser-530. We speculate that these interactions govern the binding and alignment of substrates in the cyclooxygenase channel of COX-2 and that the lack of a requirement for binding to Arg-120 and the flexibility at the aperture of the channel allow for a broader spectrum of substrates to be oxygenated. The differences observed for the 2,3-dihydroxypropyl moiety conformations of 1-AG in each monomer of the R513H:1AG crystal structure and the observed conformations of AA in each monomer of the L531F:AA crystal structure (10) lend support to this argument.

In conclusion, the crystal structure of muCOX-2 in complex with 1-AG presented here provides the first molecular insight into the productive binding of endocannabinoid substrate in the cyclooxygenase channel of COX-2. Moreover, the functional characterization of Tyr-355, Arg-513, and Leu-531 mutants coupled with structural analyses of the R513H:AA and R513H:1AG crystal structures define the roles that these residues play in high affinity binding of endocannabinoid substrates to COX-2. Finally, these structure-function studies provide additional support for our previous hypothesis that implicates the flexibility associated with the side chain of Leu-531 as being responsible for increasing the volume at the opening of the cyclooxygenase channel, subsequently allowing COX-2 to oxygenate a wide ranging array of substrates compared with COX-1.

## REFERENCES

1. Rouzer, C. A., and Marnett, L. J. (2009) *J. Lipid Res.* **50**, (suppl.) S29–S34
2. Smith, W. L., DeWitt, D. L., and Garavito, R. M. (2000) *Annu. Rev. Biochem.* **69**, 145–182
3. Funk, C. D. (2001) *Science* **294**, 1871–1875
4. Smyth, E. M., Grosser, T., Wang, M., Yu, Y., and FitzGerald, G. A. (2009) *J. Lipid Res.* **50**, (suppl.) S423–S428
5. Blobaum, A. L., and Marnett, L. J. (2007) *J. Med. Chem.* **50**, 1425–1441
6. Marnett, L. J. (2009) *Annu. Rev. Pharmacol. Toxicol.* **49**, 265–290
7. Garavito, R. M., Malkowski, M. G., and DeWitt, D. L. (2002) *Prostaglandins Other Lipid Mediat.* **68–69**, 129–152
8. Schneider, C., Pratt, D. A., Porter, N. A., and Brash, A. R. (2007) *Chem. Biol.* **14**, 473–488
9. Malkowski, M. G., Ginell, S. L., Smith, W. L., and Garavito, R. M. (2000) *Science* **289**, 1933–1937
10. Vecchio, A. J., Simmons, D. M., and Malkowski, M. G. (2010) *J. Biol. Chem.* **285**, 22152–22163
11. Yuan, C., Rieke, C. J., Rimon, G., Wingerd, B. A., and Smith, W. L. (2006) *Proc. Natl. Acad. Sci. U.S.A.* **103**, 6142–6147
12. Yuan, C., Sidhu, R. S., Kuklev, D. V., Kado, Y., Wada, M., Song, I., and Smith, W. L. (2009) *J. Biol. Chem.* **284**, 10046–10055
13. Kozak, K. R., Prusakiewicz, J. J., Rowlinson, S. W., Prudhomme, D. R., and Marnett, L. J. (2003) *Biochemistry* **42**, 9041–9049
14. Yu, M., Ives, D., and Ramesha, C. S. (1997) *J. Biol. Chem.* **272**, 21181–21186
15. Kozak, K. R., Prusakiewicz, J. J., Rowlinson, S. W., Schneider, C., and Marnett, L. J. (2001) *J. Biol. Chem.* **276**, 30072–30077
16. Kozak, K. R., Rowlinson, S. W., and Marnett, L. J. (2000) *J. Biol. Chem.* **275**, 33744–33749

17. Prusakiewicz, J. J., Kingsley, P. J., Kozak, K. R., and Marnett, L. J. (2002) *Biochem. Biophys. Res. Commun.* **296**, 612–617
18. Bisogno, T. (2008) *J. Neuroendocrinol.* **20**, (suppl.) 1–9
19. Kozak, K. R., Crews, B. C., Morrow, J. D., Wang, L. H., Ma, Y. H., Wein-  
ander, R., Jakobsson, P. J., and Marnett, L. J. (2002) *J. Biol. Chem.* **277**,  
44877–44885
20. Kozak, K. R., Crews, B. C., Ray, J. L., Tai, H. H., Morrow, J. D., and Marnett,  
L. J. (2001) *J. Biol. Chem.* **276**, 36993–36998
21. Kozak, K. R., Prusakiewicz, J. J., and Marnett, L. J. (2004) *Curr. Pharm. Des.*  
**10**, 659–667
22. Rouzer, C. A., and Marnett, L. J. (2008) *J. Biol. Chem.* **283**, 8065–8069
23. Rowlinson, S. W., Kiefer, J. R., Prusakiewicz, J. J., Pawlitz, J. L., Kozak, K. R.,  
Kalgutkar, A. S., Stallings, W. C., Kurumbail, R. G., and Marnett, L. J.  
(2003) *J. Biol. Chem.* **278**, 45763–45769
24. Rouzer, C. A., Ghebreselasie, K., and Marnett, L. J. (2002) *Chem. Phys.*  
*Lipids* **119**, 69–82
25. Dodson, E. J., Winn, M., and Ralph, A. (1997) *Methods Enzymol.* **277**,  
620–633
26. McCoy, A. J., Grosse-Kunstleve, R. W., Adams, P. D., Winn, M. D., Sto-  
roni, L. C., and Read, R. J. (2007) *J. Appl. Crystallogr.* **40**, 658–674
27. Langer, G., Cohen, S. X., Lamzin, V. S., and Perrakis, A. (2008) *Nat. Protoc.*  
**3**, 1171–1179
28. Emsley, P., and Cowtan, K. (2004) *Acta Crystallogr. D Biol. Crystallogr.* **60**,  
2126–2132
29. Murshudov, G. N., Vagin, A. A., and Dodson, E. J. (1997) *Acta Crystallogr.*  
*D Biol. Crystallogr.* **53**, 240–255
30. Schuettelkopf, A. W., and van Aalten, D. M. (2004) *Acta Crystallogr. D*  
*Biol. Crystallogr.* **D60**, 1355–1363
31. Winn, M. D., Isupov, M. N., and Murshudov, G. N. (2001) *Acta Crystal-*  
*logr. D Biol. Crystallogr.* **57**, 122–133
32. Painter, J., and Merritt, E. A. (2006) *Acta Crystallogr. D Biol. Crystallogr.*  
**62**, 439–450
33. Painter, J., and Merritt, E. A. (2006) *J. Appl. Crystallogr.* **39**, 109–111
34. Brünger, A. T., Adams, P. D., Clore, G. M., DeLano, W. L., Gros, P.,  
Grosse-Kunstleve, R. W., Jiang, J. S., Kuszewski, J., Nilges, M., Pannu, N. S.,  
Read, R. J., Rice, L. M., Simonson, T., and Warren, G. L. (1998) *Acta*  
*Crystallogr. D Biol. Crystallogr.* **54**, 905–921
35. Davis, I. W., Leaver-Fay, A., Chen, V. B., Block, J. N., Kapral, G. J., Wang,  
X., Murray, L. W., Arendall, W. B., 3rd, Snoeyink, J., Richardson, J. S., and  
Richardson, D. C. (2007) *Nucleic Acids Res.* **35**, W375–W383
36. Potterton, L., McNicholas, S., Krissinel, E., Gruber, J., Cowtan, K., Emsley,  
P., Murshudov, G. N., Cohen, S., Perrakis, A., and Noble, M. (2004) *Acta*  
*Crystallogr. D Biol. Crystallogr.* **60**, 2288–2294
37. Malkowski, M. G., Theisen, M. J., Scharmen, A., and Garavito, R. M.  
(2000) *Arch. Biochem. Biophys.* **380**, 39–45
38. Kiefer, J. R., Pawlitz, J. L., Moreland, K. T., Stegeman, R. A., Hood, W. F.,  
Gierse, J. K., Stevens, A. M., Goodwin, D. C., Rowlinson, S. W., Marnett,  
L. J., Stallings, W. C., and Kurumbail, R. G. (2000) *Nature* **405**, 97–101
39. Malkowski, M. G., Thuresson, E. D., Lakkides, K. M., Rieke, C. J., Micielli,  
R., Smith, W. L., and Garavito, R. M. (2001) *J. Biol. Chem.* **276**,  
37547–37555
40. Thuresson, E. D., Malkowski, M. G., Lakkides, K. M., Rieke, C. J., Mu-  
lichak, A. M., Ginell, S. L., Garavito, R. M., and Smith, W. L. (2001) *J. Biol.*  
*Chem.* **276**, 10358–10365
41. So, O. Y., Scarafia, L. E., Mak, A. Y., Callan, O. H., and Swinney, D. C.  
(1998) *J. Biol. Chem.* **273**, 5801–5807
42. Rieke, C. J., Mulichak, A. M., Garavito, R. M., and Smith, W. L. (1999)  
*J. Biol. Chem.* **274**, 17109–17114
43. Thuresson, E. D., Lakkides, K. M., Rieke, C. J., Sun, Y., Wingerd, B. A.,  
Micielli, R., Mulichak, A. M., Malkowski, M. G., Garavito, R. M., and  
Smith, W. L. (2001) *J. Biol. Chem.* **276**, 10347–10357
44. Shimokawa, T., and Smith, W. L. (1992) *J. Biol. Chem.* **267**, 12387–12392
45. Evans, P. (2006) *Acta Crystallogr. D Biol. Crystallogr.* **62**, 72–82